Application of Landsat TM Data to Geological Studies, Al-Khabt Area, Southern Arabian Shield

*Mohammed Yousef H. T. Qari**
Department of Geological Sciences, University College London, Gower Street, London WC1E 6BT, United Kingdom

ABSTRACT: The Al-Khabt test-area of 225 km² within the Nabitah Mobile Belt, southern Arabian Shield, was selected for application of Landsat TM data to geological studies. The major lithologies are granites, metavolcanics, metasediments, and mafic dyke rocks. Most of these rocks are of late Proterozoic age. The outcrop pattern in the area is complex due to multiple episodes of folding and faulting.

The geology of a structurally complex area which has been subjected to at least three phases of deformation, has been extended by applying various image processing techniques. Visual interpretations were made and several different types of geological maps were constructed. Image processing techniques included principal components analysis, decorrelation stretching, and edge enhancement. Lineament analysis revealed directions which can be related to regional tectonics of the Arabian Shield. The resulting interpretations were checked by geological fieldwork in the test-area.

Geological understanding of the complex evolution of the Arabian Shield will be much improved by employing remote sensing techniques and will allow much faster and accurate geological assessment of this vast region.

STUDY AREA

THE STUDY AREA (Figure 1) of 225 km² is located to the east of Abha city in the southern Arabian Shield. It was selected to test the utility of the Landsat Thematic Mapper (TM) sensor digital imagery to lithological and structural studies. The area has excellent exposure of a diverse suite of igneous and metamorphic rocks.

GEOLOGICAL SETTING

The exposed outcrop pattern of the area is complex due to folding, intense faulting, and intrusions. The major lithologies are Tertiary volcanic rocks, and Precambrian metamorphic and plutonic rocks. The area was mapped by Stoeser (1984) and an extract from this map, covering the study area, is shown in Figure 2.

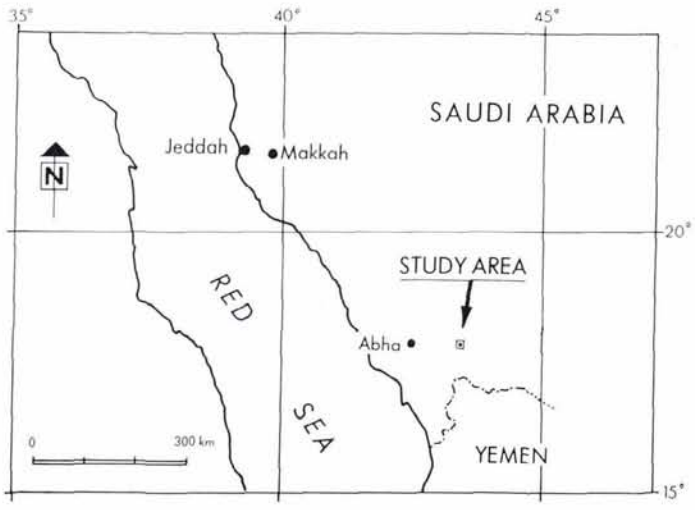

FIG. 1. Location map of the study area.

The volcanic rocks are situated in the west of the area overlying the Suwaydah tonalite gneiss. They are Tertiary alkali-olivine basalt flows of the As-Sarat mountains. The base of the basalt sequence is marked by a well-developed sub-lateritic paleosol. The metamorphic rocks occupy a small area and are well-foliated Upper Proterozoic metasedimentary rocks assigned to the Halaban Group. The plutonic rocks include granite, tonalite, gneiss, and gabbro.

A major group of east-west striking faults is shown on this map, and individual faults extend in some cases for distances of over 20 km. These are mostly right-lateral strike-slip faults and commonly have mafic dykes emplaced along portions of their length. The dykes are fine grained hornblende dolerites (Stoeser, 1984).

LANDSAT DIGITAL DATA ANALYSIS AND RESULTS

The TM scanner records six band of reflected visible and infrared light (0.45 to 2.35 μm), each picture element (pixel) measuring 30 m by 30 m on the ground, plus one thermal infrared band (10.4 to 12.5 μm), 120 m by 120 m on the ground. A Landsat TM scanner image from the Arabian winter season (1 Mar 1984, Path 167, Row 047) was obtained for the purpose of the present study, with a sun elevation angle of 57° and a sun azimuth angle of 101°. The sub-scene (Plate 1A) for the selected test-area is 512 by 512 pixels in size, which is approximately 15 by 15 kilometres.

The spectral distribution of reflected sunlight from an earth material, when represented as a tone or color in image, is invaluable for geological interpretations. The sub-scene was analyzed using various image processing techniques which included principal components analysis, decorrelation stretching, and edge enhancement. Visual interpretations were made and several different types of geological maps were constructed. Subsequently, two-days fieldwork was carried out in the test-area to measure geological elements, and to characterize mapped contacts and different lithologies.

PRINCIPAL COMPONENTS ANALYSIS

Principal components analysis (PCA) is used in various applications including remote sensing (e.g., Blodget *et al.*, 1978). Typically, for any pixel in a multispectral original image, the

*Presently with the Faculty of Earth Sciences, King Abdulaziz University, P. O. Box 1744, Jeddah 21441, Saudi Arabia.

PHOTOGRAMMETRIC ENGINEERING & REMOTE SENSING,
Vol. 57, No. 4, April 1991, pp. 421–429.

0099-1112/91/5704–421$03.00/0

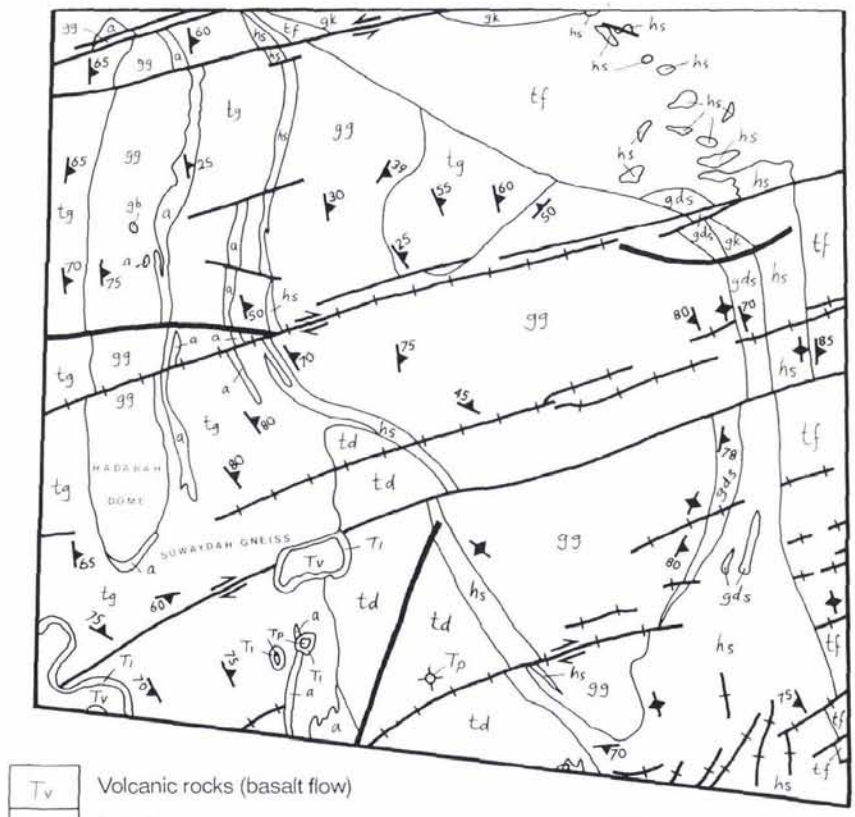

FIG. 2. Geological map (after Stoeser, 1984).

brightness values or Digital Numbers (DNs) are highly correlated from band to band, so that there is much redundancy in the data set.

PCA is used to compress multichannel image data by calculating a new coordinate system, so as to condense the scene variance in the original data into a new set of variables which are called principal components (PCs). These data are decorrelated and most of the image variance is confined within the first few channels. In this study, after transformation, the data were scaled or linearly contrast stretched. This procedure increases the spectral discrimination capability among terrestrial materials.

PCA of the Landsat TM data for the Al-Khabt test-area was applied on the six non-thermal bands (7,5,4,3,2, and 1), and a set of three-band PC color composites was created. Visual inspection of the PC color composites indicated that the composite containing the first three PCs was the most informative. This is shown with -PC1 = red, -PC2 = green, and -PC3 = blue in Plate 1B.

The basaltic rocks in the southwestern corner of the test-area display red hues, due to high albedo in the -PC1 image (section A8, Plate 1B). Because these rocks are the extension of the basaltic flows of the As-Sarat volcanic field (located to the west outside the test-area, and is high in elevation), the material transported to most of the wadis in the test-area is of basaltic composition and is displayed as a red color filling these wadis (e.g., sections A4, B7, and G7, Plate 1B). Where the alluvium in the wadis is not of basaltic composition, the color is not red (e.g., sections E2, G6, and I2, Plate 1B). Obvious contacts were detected on the -PC color composite image between most of the lithologies, such as the Hadabah dome granodioritic gneiss, the layered metamorphic rocks, and the northern granitic unit. The layered metamorphic rocks (LMR) were identified in the -PC color

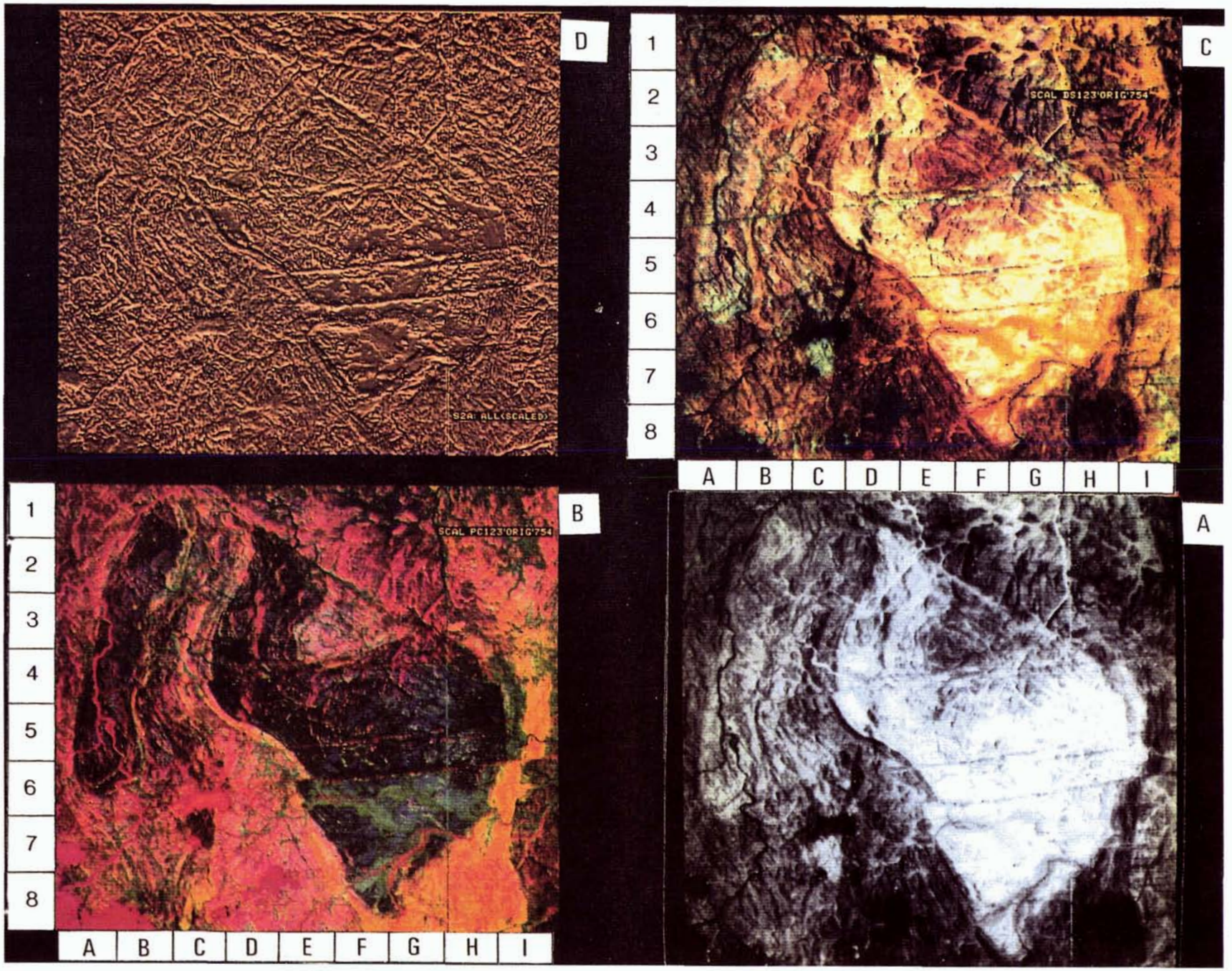

PLATE 1. (A) TM-band 5 sub-scene for the study area (15 by 15 km across); (B) -PC color composite; (C) DS color composite; (D) High-pass filtered image, (see text for details).

composite as yellow hues, particularly in the eastern flank of the Al-Khabt synformal phacolith (e.g, sections G8 and H8, Plate 1B). These LMR also appear in the eastern part of the Hadabah dome and in the southwestern corner of the area next to the basaltic rocks (section C8, Plate 1B). Small patches of these LMR are easily distinguished within the northern granitic unit as yellow patches in pinkish color (granite). The granitoid rocks in the test-area, which include granites, tonalites, and granodiorite- and tonalite-gneisses can be distinguished as two groups. The granodioritic composition (Hadabah dome and Al-Khabt synformal phacolith) display a blue color, while the other group which displays pink hues includes the northern granite, Suwaydah tonalite gneiss, and mafic tonalites. The mafic dyke rocks filling the east-west faults are also identifiable as red colors cutting through the blue and pink colors of assorted lithologies, particularly in the Al-Khabt phacolith (e.g., sections D4 and F6, Plate 1B). Because the Al-Khabt synformal phacolith granodioritic gneiss includes tonalite gneiss, it also can be distinguished on the -PC color composite as a pink color (section F3, Plate 1B).

Decorrelation Stretching

Another way of emphasizing spectral information in an image is decorrelation stretching (DS). DS serves to exaggerate color differences which may be very subtle in the raw or scaled color composite. Generally, color saturation is increased without significant distortion of the hue.

The DS transformation involves using the original eigen vector matrix of the PCA in order to create a DS image by transformation of the PCs back to the domain of the original variables. Displaying the manipulated variables in red, green, and blue color space retains the color appearance of the original three-channel false color image and the useful topographic information (e.g., Gillespie *et al.*, 1986; Rothery, 1987).

The TM band 7,5,4 red, green and blue DS color composite image of the Al-Khabt test-area is shown in Plate 1C. The basaltic rocks in the southwestern corner of the test-area display blue hues (section A8, Plate 1C), which should not be confused with the blue color along some wadis which are material transported from the As-Sarat volcanic flow to the west of the test-area. The sub-lateritic paleosol is easily identifiable in the DS color composite as light-blue color rims of the basaltic rocks (e.g., sections B8, Plate 1C). The granitoid rocks are shown mostly in bright-white hues mixed with a brown color, although one can distinguish the Hadabah dome- and the Al-Khabt synformal phacolitic-granodioritic gneisses from other granitoid lithologies. The layered metamorphic rocks are not as easily identifiable as in the -PC color composite, though brownish in color (e.g., section G8, Plate 1C). The mafic dyke rocks which intrude the E-W faults are also very distinctive (e.g., sections G6 and H4, Plate 1C).

A detailed geological map of the Al-Khabt test-area was constructed (Figure 3) from the DS color composite taking advantage also of information from the principal components analysis composite image. Field observations were used extensively to supplement remote sensing interpretations, particularly in the northern granitic unit. Comparing with the geological information contained in the earlier map (Figure 2), it is clear that, although there is a good correspondence between the two maps, there is more detail in the TM-based map. The area which was mapped as Al Fayd tonalite in the previous map can be resolved into two lithologies, which are the Al Fayd tonalite and the northern granitic unit. In addition, the schistose rocks were mapped easily within the granitic unit in the northeast quarter of the map (Figure 3).

The Al Fayd tonalite and the northern granitic unit are showing as greenish and pinkish hues in the -PC composite image, respectively. In the field, the tonalite is gneissose uniform body rich in hornblende and light- to medium-grey in color, whereas granite is rich in biotite and pinkish in color. The tonalite is locally migmatized near the contact with the granite.

Edge Enhancement

Edge enhancement was achieved by high-pass filtering, emphasizing higher spatial frequencies, using a convolution operation to increase lineament contrast. TM band 5 (1.55 to 1.75 μm) was selected, and a simple unsymmetrical weighted kernel of size 3 by 3 pixels was applied. The resultant filtered image is shown in Plate 1D, which allowed the drawing of the lineaments or fractures. However, an even better image was obtained by adding this scaled image to the original TM band 5 image which is shown in Plate 2.

The lineaments were identified by visual inspection and recorded on a transparent overlay as ruled lines. A remotely sensed lineament map was constructed (Figure 4) based on the total knowledge compiled from edge enhancement, principal components, and decorrelation stretech images together with the ground study. In identifying lineaments, what remains relatively constant represents the azimuth and the length of a line rather than its precise location. The fracture map shows that lineament frequency is generally constant within the test-area. The significance of the interpreted lineaments was analyzed using histograms (Figure 5). Figure 5A shows strike-frequency distribution and length of lineaments in the test-area. There is a single dominant preferred orientation of lineaments in the west direction; however, there are general concentrations at NW-SE and ENE-WSW directions. There is a good correspondence between the length of these lineaments and their distribution, but when both distribution and length were plotted to percentage (Figure 5B), one can compare the distribution of lineaments with their length, except in the west direction where length of lineaments is much higher, which represents the long faults which were filled with mafic dyke rocks in the test-area. Frequency and length of these lineaments were plotted against each other; the scatter of points is confined to the lower diagonal half of the diagram (Figure 6), though a positive good correlation is obtainable.

The lineaments shown on Figure 4 were counted on a 2.5- by 2.5-km grid and the total density contoured (Figure 7) to examine the pattern of concentration. The number of lineaments/6.25 km^2 varies from 3 to 21. Several concentrations of lineaments are quite apparent throughout the test-area, particularly in the Al-Khabt synformal phacolith area.

Comparison of observed lineaments with previously mapped features showed that many of them coincide with mapped faults. However, about 60 percent correspond to joint sets that have not previously been mapped in ground surveys.

STRUCTURES

An attempt to construct a structural map (Figure 8) was based on color composites, field studies, correlation with detailed ground studies of comparable areas (Amlas, 1983; Qari, 1985), and the available work of Stoeser (1984).

As in other regions nearby (Amlas, 1983; Qari, 1985, 1989), all rock units and in particular the layered metamorphic rocks exhibit well developed S_1 to S_2 foliation. This axial planar foliation is a strongly developed fabric and easily distinguishable as schistosity or fracture cleavage across minor F_2 fold hinges. The foliation is broadly parallel to the contacts between the lithologies throughout the test-area. This foliation is amlost parallel to S_1 foliation and thus difficult to distinguish from S_1 foliation. The S_2 foliation generally strikes between north and northeast and it is folded around the hinges of later fold generations.

The F_2 folds are present in the limbs of the F_3 major folds, particularly in the layered metamorphic rocks in the southeast

PLATE 2. Directionally enhanced image superimposing TM-band 5 for the study area.

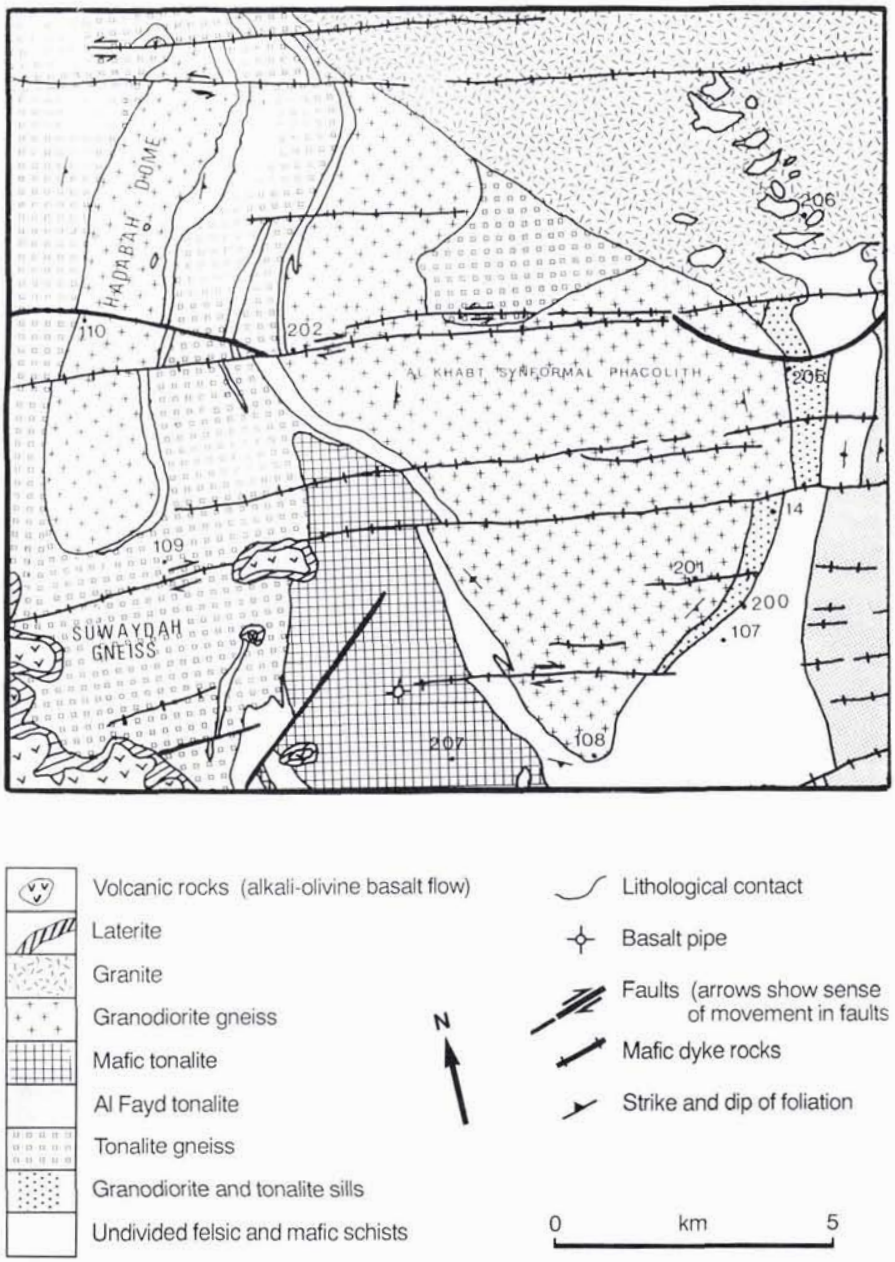

FIG. 3. Geological map constructed from the color composites. Numbers indicate 11 localities visited.

quarter of the test-area. The F_2 phase is represented by tight, upright asymmetrical folds where the axial planes are parallel to the S_2 foliation.

F_3 folds are the most dominant and widespread structures and defining the major structures of Al-Khabt test-area. This phase is found as tight- to open-asymmetrical folds with variable geometry. Three major antiforms and synforms with steep, generally north-south axial planes, and plunging towards south in the test-area, are assigned to F_3 folds (Figure 8). The Hadabah dome is the result of two antiforms found plunging in opposite directions. Linear structures associated with F_3 folding were observed around the hinge of Al-Khabt synform as a strong mineral lineation in the schistose rocks trending mostly towards south with low to moderate plunges, which is in correspondence with the plunge of the synform.

Faults are very prominent in the Al-Khabt test-area. They are easily detectable on the color composites. Most of these east-west faults are right-lateral strike-slip faults intruded by mafic dyke rocks. Some of these faults can be traced into the Tertiary As-Sarat volcanic field which suggests that they may have been rejuvenated during the Tertiary (Stoeser, 1984).

CONCLUSIONS

The Al-Khabt test-area within the southern Arabian Shield was selected for the evaluation of the Landsat TM data for geological studies. Principal components analysis, decorrelation stretching, and edge enhancement techniques were used for mapping different lithologies and for the structural analysis of this rugged terrain. Sharp lithological boundaries based on color composites were easily detectable which was checked by field-

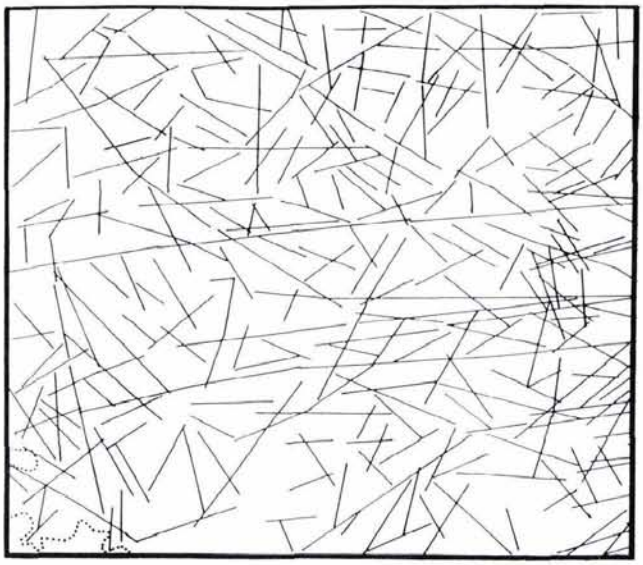

FIG. 4. Remotely sensed lineament map.

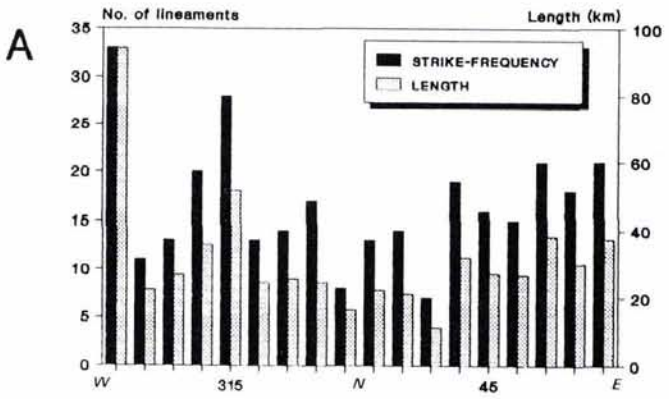

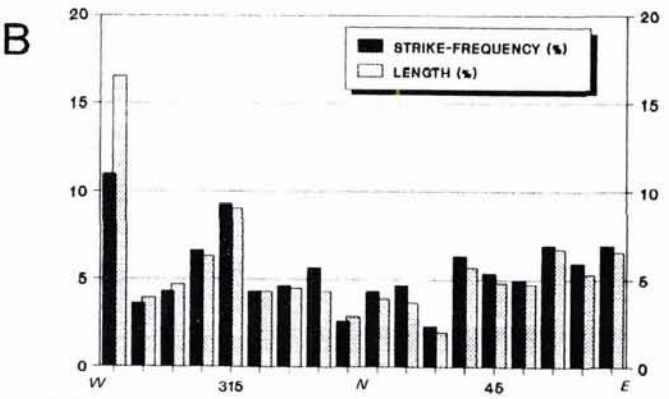

FIG. 5. Histograms summarizing 301 lineaments in Figure 4, (see text for details).

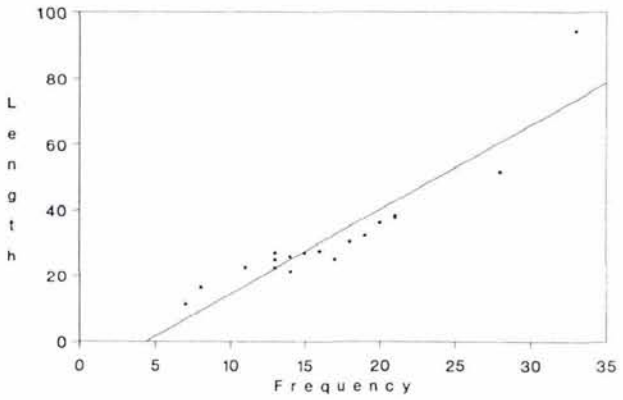

FIG. 6. Cross-plot of frequency versus length for lineaments in the study area.

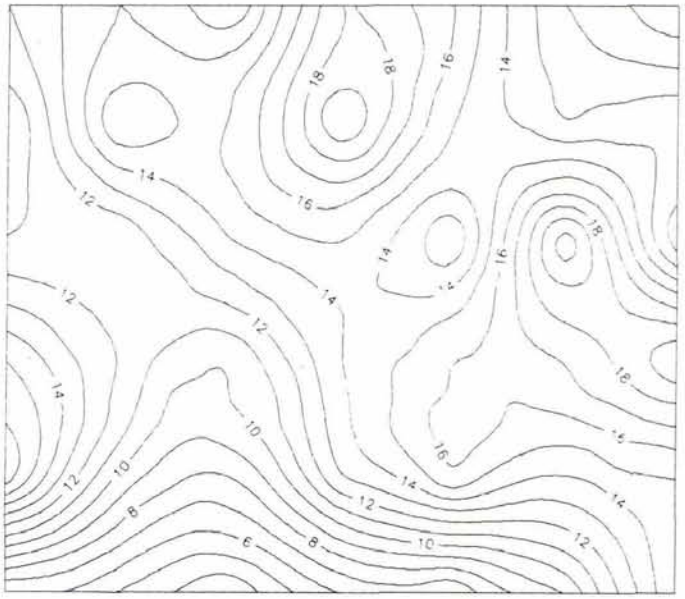

FIG. 7. Fracture density isopleth map. Fracture density is expressed in number of fractures/6.25 km^2.

work, and hence utilized in preparing the geological map of the test-area.

At least three phases of deformation (D_1, D_2, and D_3) have affected the area; however, the dominant and major structures in the test-area are the D_3 structures. This third phase of folding is asymmetrical, tight-to-open, and plunging generally towards south. L_3 lineation is developed, in general, parallel to the fold axes of F_3. Faulting is also very prominent.

Quantitative examination of the lineaments showed that the test-area has several significant preferred directions; these are E-W, NW-SE, and ENE-WSW. Length of these lineaments is comparable with their distribution, except in the west directin where it is reflecting the obvious long E-W faults filled with mafic dyke rocks.

The NW-SE direction is proposed to be part of the Najd fault system which had affected the Arabian Shield at about 530 to 630 Ma (Moore, 1979), whereas the E-W direction is conformable with the older east-trending tectonic fabric in the tectonically more complex and possibly older parts of the shield which was postulated by Moore (1983). The general NE-SW or ENE-WSW direction is postulated to be the youngest, possibly the exten-

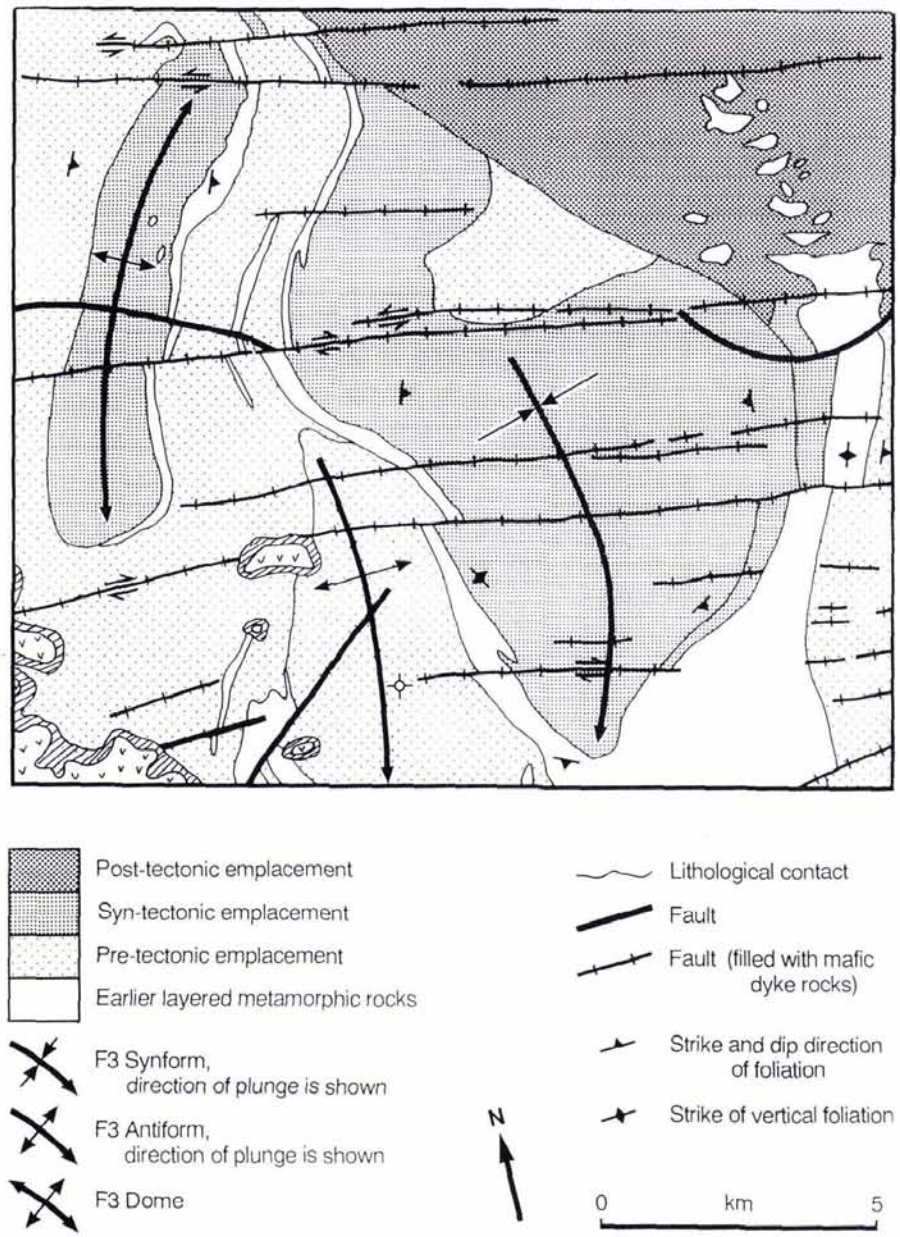

FIG. 8. Structural map constructed from the color composites, field work, and Stoeser (1984).

sion of transform faults identified in the Red Sea by several geophysical surveys (ARGAS, 1977), or the signature of a conjugate set of fractures developed at the same time with the Najd system.

Results show that TM data can be used reliably for lithological and structural studies in well exposed arid regions. The combination of image processing techniques and fieldwork permits the construction of better geological maps.

ACKNOWLEDGMENTS

This paper is based partly on a Ph.D. research project at University College London (UCL), which is sponsored by the King Abdulaziz University (KAAU), Jeddah, Saudi Arabia. I am grateful to Dr. R. Mason, for discussions in the field, and to Dr. R. Hall, for his helpful comments and reading the manuscript. Thanks are also due to Dr. M. Tawfiq, Saudi Arabian Directorate General of Mineral Resources, Jeddah, for providing the digital imagery, and Drs. F. Zakir and P. Chagarlamudi of KAUU, for helping in producing the hard copies. The imagery was enhanced using the IIS interactive image processing system in the Department of Geography at UCL. This paper has benefitted from comments by Dr. D. Rothery, Open University, U.K., and three anonymous reviewers.

REFERENCES

Amlas, M. M. A., 1983. *Geology and Structures of the Precambrian Rocks North of Khamis Mushayt, Southern Arabian Shield.* M.Sc. thesis, Faculty of Earth Sciences, King Abdulaziz Univ., Jeddah, Saudi Arabia.

ARGAS, 1977. *Geophysical Synthesis Report, Eastern Part of the Central Red Sea.* Saudi-Sudanese Commission for the Exploitation of the Red Sea Resources.

Blodget, H. W., F. J. Gunther, and M.H. Podwysocki, 1978. *Discrimi-*

nation of Rock Classes and Alteration Products in Southwestern Saudi Arabia with Computer-Enhanced Landsat Data. NASA Technical Paper 1327.

Gillespie, A. R., A. B. Kahle, and R. E. Walker, 1986. Color enhancement of highly correlated images. I. Decorrelation and HSI contrast stretches. *Remote Sensing of Environment,* 20:209–235.

Moore, J. M., 1979. Tectonics of the Najd transcurrent fault system, Saudi Arabia. *J. Geol. Soc. London,* 136:441–454.

———, 1983. *Tectonic Fabric and Structural Control of Mineralization in the Southern Arabian Shield: A Compilation Based on Satellite Imagery Interpretation.* Saudi Arabian Deputy Ministry for Mineral Resources Open-File Report USGS-OF-03-105.

Qari, M. Y. H. T., 1985. *Structural Analysis of the Proterozoic Rocks Near Janfoor Village (Northwest of Khamis Mushayt), Southern Arabian Shield.* M.Sc. thesis, Faculty of Earth Sciences, King Abdulaziz Univ., Jeddah, Saudi Arabia.

———, 1989. Lithological mapping and structural analysis of Proterozoic rocks in part of the southern Arabian Shield using Landsat images. *Int. J. Remote Sensing,* 10:499–503.

Rothery, D.A., 1987. Improved discrimination of rock units using Landsat Thematic Mapper imagery of the Oman ophiolite. *J. Geol. Soc. London,* 144:587–597.

Stoeser, D. B., 1984. *Reconnaissance Geology of the Wadi Tarib Quadrangle, Kingdom of Saudi Arabia.* Saudi Arabian Deputy Ministry for Mineral Resources Technical Record USGS-TR-04-4.

(Received 19 March 1990; revised and accepted 1 August 1990)

Forthcoming Articles

K. F. Adkins and *J. G. Lyon,* Use of Aerial Photographs to Identify Suitable GPS Survey Stations.

Eric W. Augenstein, Douglas A. Stow, and *Allen S. Hope,* Evaluation of SPOT HRV-XS Data for Kelp Resource Inventories.

Emmanuel P. Baltsavias and *Dirk Stallmann,* Trinocular Vision for Automatic and Robust Three-Dimensional Determination of the Trajectories of Moving Objects.

Eugenia M. Barnaba, Warren R. Philipson, Arlynn W. Ingram, and *Jim Pim,* The Use of Aerial Photographs in County Inventories of Waste-Disposal Sites.

Jon S. Beazley, What is this Thing Called Ethics and, Sometimes, The Code of Ethics?

D. S. Bhargava and *Dejene W. Mariam,* Effects of Suspended Particle Size and Concentration on Reflectance Measurements.

Michel Boulianne, Louis Cloutier, and *Sanjib K. Ghosh,* Cerebral Biopsies Using a Photogrammetric Probe Simulator.

Doug C. Brockelbank and *Ashley P. Tam,* Stereo Elevation Determination Techniques for SPOT Imagery.

Jeffrey D. Colby, Topographic Normalization in Rugged Terrain.

Heinrich Ebner, Wolfgang Kornus, Gunter Strunz, Otto Hofmann, and *Franz Muller,* A Simulation Study on Point Determination Using MOMS-02/D2 Imagery.

W. Frobin and *E. Hierholzer,* Video Rasterstereography: A Method for On-Line Measurement of Body Surfaces.

Sanjib K. Ghosh and *Zhengdong Shi,* Evaluating Dynamic Performance of an Analytical Plotter.

Peng Gong and *J. Douglas Dunlop,* Comments on the Skidmore and Turner Supervised Nonparametric Classifier (and response).

Joshua S. Greenfeld, An Operator-Based Matching System.

Nils N. Haag, Michael H. Brill, and *Eamon B. Barrett,* Invariant Relationships in Side-Looking Synthetic Aperture Radar Imagery.

Peter E. Joria, Sean C. Ahearn, and *Michael Conner,* A Comparison of the SPOT and Landsat Thematic Mapper Satellite Systems for Detecting Gypsy Moth Defoliation in Michigan.

Brenton J. Keefer, James L. Smith, and *Timothy G. Gregoire,* Modeling and Evaluating the Effects of Stream Mode Digitizing Errors on Map Variables.

T. K. Koo and *Y. B. Aw,* A Three-Dimensional Visualization Approach to Traffic Accident Mapping.

J. Lavreau, De-Hazing Landsat Thematic Mapper Images.

Hans Middelkoop and *Lucas L. F. Janssen,* Implementation of Temporal Relationships in Knowledge-Based Classification of Satellite Images.

A. J. Naftel and *J. C. Boot,* An Iterative Linear Transformation Algorithm for Solution of the Collinearity Equations.

William R. Niedzwiedz and *Lee W. Ganske,* Assessing Lakeshore Permit Compliance Using Low Altitude Oblique 35-mm Aerial Photography.

J. Raul Ramirez, Digital Topographic Maps: Production Problems and Their Impact on Quality and Cost.

Michael Rast, Simon J. Hook, Christopher D. Elvidge, and *Ronald E. Alley,* An Evaluation of Techniques for the Extraction of Mineral Absorption Features from High Spectral Resolution Remote Sensing Data.

Randall L. Repic, Jae K. Lee, Paul W. Mausel, David E. Escobar, and *James H. Everitt,* An Analysis of Selected Water Parameters in Surface Coal Mines Using Multi-spectral Videography.

Eric J. M. Rignot, Ronald Kwok, John C. Curlander, and *Shirley S. Pang,* Automated Multisensor Registration: Requirements and Techniques.

T. W. Ryan, P. Sementilli, P. Yuen, and *B. R. Hunt,* Extraction of Shoreline Features by Neural Nets and Image Processing.

*Toni Schenk, Jin-Cheng Li,*D and *Charles Toth,* Towards an Autonomous System for Orienting Digital Stereopairs.

Jayanta K. Sircar and *Juan A. Cebrian,* An Automated Approach for Labeling Raster Digitized Contour Maps.

S. D. Wall, T. G. Farr, J -P Muller, P. Lewis, and *F. W. Leberl,* Measurement of Surface Microtopography.